

# On the implementation of the $k - \varepsilon$ turbulence model in incompressible flow solvers based on a finite element discretization

**D. Kuzmin\***

Institute of Applied Mathematics (LS III)  
University of Dortmund, Dortmund, Germany  
E-mail: kuzmin@math.uni-dortmund.de  
\*Corresponding author

**O. Mierka**

Institute of Applied Mathematics (LS III)  
University of Dortmund, Dortmund, Germany  
E-mail: omierka@math.uni-dortmund.de

**S. Turek**

Institute of Applied Mathematics (LS III)  
University of Dortmund, Dortmund, Germany  
E-mail: stefan.turek@math.uni-dortmund.de

**Abstract:** A finite element implementation of the standard  $k - \varepsilon$  turbulence model including Chien's Low-Reynolds number modification is presented. The incompressible Navier-Stokes equations are solved using an extension of the in-house software package FEATFLOW (<http://www.featflow.de>). Algebraic flux correction based on a multidimensional flux limiter of TVD type (Kuzmin and Turek, 2004) is invoked to suppress nonphysical oscillations produced by the *a priori* unstable Galerkin discretization of convective terms. A block-iterative algorithm based on a hierarchy of nested loops is employed to advance the solution in time. Special emphasis is laid on the numerical treatment of wall boundary conditions. In particular, logarithmic wall functions are used to derive Neumann boundary conditions for the standard  $k - \varepsilon$  model. The resulting solutions are superior to those obtained using wall functions implemented as Dirichlet boundary conditions and comparable to simulation results produced by a Low-Reynolds number  $k - \varepsilon$  model. Two representative benchmark problems (channel flow and backward facing step) are used to compare the performance of different algorithms in 3D and to investigate the influence of the near-wall treatment.

**Keywords:** Navier-Stokes equations,  $k - \varepsilon$  turbulence model, wall boundary conditions

---

## 1 INTRODUCTION

---

Turbulence plays an important role in many chemical engineering processes (fluid flow, mass and heat transfer, chemical reactions) which are dominated by convective transport. Since the direct numerical simulation (DNS) of turbulent flows is still prohibitively expensive, eddy viscosity models based on the Reynolds Averaged Navier-Stokes (RANS) equations are commonly employed in CFD codes. One of the most popular ones is the standard  $k - \varepsilon$  model which has been in use since the 1970s. However, its prac-

tical implementation and, especially, the near-wall treatment has always been somewhat of a mystery. Algorithmic details and employed 'tricks' are rarely reported in the literature, so that a novice to this area of CFD research often needs to reinvent the wheel. The numerical implementation of turbulence models involves many algorithmic components all of which may have a decisive influence on the quality of simulation results. In particular, a positivity-preserving discretization of the troublesome convective terms is an important prerequisite for the robust-

Copyright © 200x Inderscience Enterprises Ltd.

ness of the numerical algorithm. This paper presents a detailed numerical study of the  $k - \varepsilon$  model as implemented in an unstructured grid finite element code. The proposed algorithm combines and extends some useful ideas found in the literature (Grotjans and Menter, 1998; Codina and Soto, 1999; Medić and Mohammadi, 1999; Lew et-al., 2001). The main highlight is a new formulation of logarithmic wall functions, whereby the boundary conditions for  $k$  and  $\varepsilon$  are prescribed in a weak sense using a fixed value of the parameter  $y^+$ . The resulting solutions are in a good agreement with those produced by Chien’s Low-Re  $k - \varepsilon$  model, as demonstrated by numerical examples.

## 2 IMPLEMENTATION OF THE $k - \varepsilon$ MODEL

### 2.1 Mathematical model

In the framework of eddy viscosity models, the flow of a turbulent incompressible fluid is governed by the RANS equations for the velocity  $\mathbf{u}$  and pressure  $p$

$$\begin{aligned} \frac{\partial \mathbf{u}}{\partial t} + \mathbf{u} \cdot \nabla \mathbf{u} &= -\nabla p + \nabla \cdot ((\nu + \nu_T)[\nabla \mathbf{u} + \nabla \mathbf{u}^T]), \\ \nabla \cdot \mathbf{u} &= 0, \end{aligned} \quad (1)$$

where the kinematic viscosity  $\nu$  depends only on the physical properties of the fluid, while  $\nu_T$  is the turbulent eddy viscosity which is supposed to emulate the effect of unresolved velocity fluctuations  $\mathbf{u}'$ .

The standard  $k - \varepsilon$  model is based on the assumption that  $\nu_T = C_\mu \frac{k^2}{\varepsilon}$ , where  $k$  is the turbulent kinetic energy and  $\varepsilon$  is the dissipation rate. Hence, the above PDE system is to be complemented by two additional convection-diffusion-reaction equations for computation of  $k$  and  $\varepsilon$

$$\frac{\partial k}{\partial t} + \nabla \cdot \left( k \mathbf{u} - \frac{\nu_T}{\sigma_k} \nabla k \right) = P_k - \varepsilon, \quad (2)$$

$$\frac{\partial \varepsilon}{\partial t} + \nabla \cdot \left( \varepsilon \mathbf{u} - \frac{\nu_T}{\sigma_\varepsilon} \nabla \varepsilon \right) = \frac{\varepsilon}{k} (C_1 P_k - C_2 \varepsilon), \quad (3)$$

where  $P_k = \frac{\nu_T}{2} |\nabla \mathbf{u} + \nabla \mathbf{u}^T|^2$  and  $\varepsilon$  are responsible for production and dissipation of turbulent kinetic energy, respectively. The default values of the involved empirical constants are as follows:  $C_\mu = 0.09$ ,  $C_1 = 1.44$ ,  $C_2 = 1.92$ ,  $\sigma_k = 1.0$ ,  $\sigma_\varepsilon = 1.3$ . The choice of initial/boundary conditions for equations (1)–(3) will be discussed later.

### 2.2 Iterative solution strategy

The discretization in space is performed by an unstructured grid finite element method. The incompressible Navier-Stokes equations are discretized using the nonconforming  $\tilde{Q}_1/Q_0$  element pair, whereas standard  $Q_1$  elements are employed for  $k$  and  $\varepsilon$ . After an implicit time discretization by the Crank-Nicolson or backward Euler method, the nodal values of  $(\mathbf{v}, p)$  and  $(k, \varepsilon)$  are updated in a segregated fashion within an outer iteration loop.

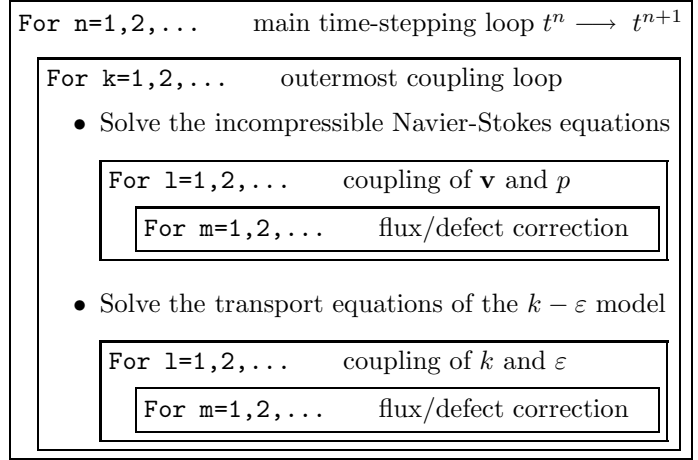
For practical implementation purposes, it is worthwhile to introduce an auxiliary parameter  $\gamma = \frac{\varepsilon}{k}$ , so as to decouple/linearize the equations of the  $k - \varepsilon$  model using the following equivalent representation (Lew et-al., 2001)

$$\frac{\partial k}{\partial t} + \nabla \cdot \left( k \mathbf{u} - \frac{\nu_T}{\sigma_k} \nabla k \right) + \gamma k = P_k, \quad (4)$$

$$\frac{\partial \varepsilon}{\partial t} + \nabla \cdot \left( \varepsilon \mathbf{u} - \frac{\nu_T}{\sigma_\varepsilon} \nabla \varepsilon \right) + C_2 \gamma \varepsilon = \gamma C_1 P_k. \quad (5)$$

This trick leads to a positivity-preserving linearization of the troublesome sink terms, whereby the parameters  $\nu_T$  and  $\gamma$  are evaluated using the solution from the previous outer iteration (Kuzmin and Turek, 2004).

The iterative solution process is based on the following hierarchy of nested loops



At each time step (one  $n$ -loop iteration), the governing equations are solved repeatedly within the outer  $k$ -loop which contains the two subordinate  $l$ -loops responsible for the coupling of variables within the corresponding subproblem. The embedded  $m$ -loops correspond to iterative flux/defect correction for the involved convection-diffusion operators. Flux limiters of TVD type are activated in the vicinity of steep gradients, where nonlinear artificial diffusion is required to suppress nonphysical undershoots and overshoots. In the case of an implicit time discretization, subproblem (4)–(5) leads to a sequence of algebraic systems of the form (Kuzmin and Möller, 2005; Kuzmin and Turek, 2004; Turek and Kuzmin, 2005)

$$\begin{aligned} A(\mathbf{u}^{(k)}, \gamma^{(l)}, \nu_T^{(k)}) \Delta \mathbf{u}^{(m+1)} &= \mathbf{r}^{(m)}, \\ \mathbf{u}^{(m+1)} &= \mathbf{u}^{(m)} + \omega \Delta \mathbf{u}^{(m+1)}, \end{aligned} \quad (6)$$

where  $\mathbf{r}^{(m)}$  is the defect vector and the superscripts refer to the loop in which the corresponding variable is updated. The predicted values  $k^{(l+1)}$  and  $\varepsilon^{(l+1)}$  are used to recompute the linearization parameter  $\gamma^{(l+1)}$  for the next outer iteration (if any). The associated eddy viscosity  $\nu_T$  is bounded from below by a certain fraction of the laminar viscosity  $0 < \nu_{\min} \leq \nu$  and from above by  $\nu_{\max} = l_{\max} \sqrt{k}$ , where  $l_{\max}$  is the maximum admissible mixing length (the size of the largest eddies, e.g., the width of the domain).

Specifically, we define the limited mixing length  $l_*$  as

$$l_* = \begin{cases} C_\mu \frac{k^{3/2}}{\varepsilon} & \text{if } C_\mu k^{3/2} < \varepsilon l_{\max} \\ l_{\max} & \text{otherwise} \end{cases} \quad (7)$$

and calculate the turbulent eddy viscosity from the formula

$$\nu_T = \max\{\nu_{\min}, l_* \sqrt{k}\}. \quad (8)$$

The corresponding linearization parameter  $\gamma$  is given by

$$\gamma = C_\mu \frac{k}{\nu_T}. \quad (9)$$

The above representation makes it possible to preclude division by zero and obtain bounded nonnegative coefficients without manipulating the actual values of  $k$  and  $\varepsilon$ .

### 2.2.1 Initial conditions

As a rule, it is rather difficult to devise a reasonable initial guess for a steady-state simulation or proper initial conditions for a dynamic one. If the velocity field is initialized by zero, it takes the flow some time to become fully turbulent. Therefore, the  $k - \varepsilon$  model is activated at a certain time  $t_* > 0$  after the startup. During the ‘laminar’ initial phase ( $t \leq t_*$ ), a constant effective viscosity  $\nu_0 = \mathcal{O}(\nu)$  is prescribed. The values to be assigned to  $k$  and  $\varepsilon$  at  $t = t_*$  depend on the choice of  $\nu_0$  and of the default mixing length  $l_0 \in [l_{\min}, l_{\max}]$  where the threshold parameter  $l_{\min}$  corresponds to the size of the smallest admissible eddies

$$k_0 = \left(\frac{\nu_0}{l_0}\right)^2, \quad \varepsilon_0 = C_\mu \frac{k_0^{3/2}}{l_0} \quad \text{at } t \leq t_*. \quad (10)$$

Alternatively, the initial values of  $k$  and  $\varepsilon$  can be estimated by means of a zero-equation (mixing length) model or computed using an extension of the inflow or wall boundary conditions (see below) into the interior of the domain.

### 2.2.2 Boundary conditions

At the inflow boundary  $\Gamma_{\text{in}}$ , all velocity components as well as the values of  $k$  and  $\varepsilon$  are to be prescribed:

$$\mathbf{u} = \mathbf{g}, \quad k = c_{bc} |\mathbf{u}|^2, \quad \varepsilon = C_\mu \frac{k^{3/2}}{l_0} \quad \text{on } \Gamma_{\text{in}}, \quad (11)$$

where  $c_{bc} \in [0.003, 0.01]$  is an empirical constant and  $|\mathbf{u}| = \sqrt{\mathbf{u} \cdot \mathbf{u}}$  is the Euclidean norm of the velocity. At the outlet  $\Gamma_{\text{out}}$ , the normal gradients of all variables are set equal to zero. This corresponds to the homogeneous Neumann (‘do-nothing’) boundary condition which implies that the surface integrals resulting from integration by parts in the variational formulation vanish

$$\begin{aligned} \mathbf{n} \cdot [\nabla \mathbf{u} + \nabla \mathbf{u}^T] &= 0, \\ \mathbf{n} \cdot \nabla k &= 0, \quad \mathbf{n} \cdot \nabla \varepsilon = 0 \end{aligned} \quad \text{on } \Gamma_{\text{out}}. \quad (12)$$

At an impervious solid wall  $\Gamma_w$ , the normal component of the velocity is set equal to zero

$$\mathbf{n} \cdot \mathbf{u} = 0 \quad \text{on } \Gamma_w, \quad (13)$$

whereas tangential slip is permitted in turbulent flow simulations. The practical implementation of the above ‘free-slip’ condition is nontrivial if the boundary of the computational domain is not aligned with the axes of the Cartesian coordinate system. In this case, condition (13) is imposed on a linear combination of several velocity components whereas their boundary values are unknown. Therefore, standard implementation techniques based on a modification of the corresponding matrix rows cannot be used.

In the FEM framework, the free-slip condition is typically implemented using element-by-element transformations to a local coordinate system spanned by the normal and tangential vectors (Engelman et-al, 1982). However, this strategy requires substantial modifications of the finite element code. An easier way to set the normal velocity component equal to zero was introduced in (Kuzmin and Turek, 2004; Turek and Kuzmin, 2005). The crux is to nullify the off-diagonal entries of the preconditioner  $A(\mathbf{u}^{(m)}) = \{a_{ij}^{(m)}\}$  in the defect correction loop for the momentum equation. As a result, the boundary values of the velocity vector  $\mathbf{u}$  can be calculated explicitly before solving the linear system for the remaining degrees of freedom:

$$\begin{aligned} a_{ij}^{(m)} &:= 0, \quad \forall j \neq i, \\ \mathbf{u}_i^* &:= \mathbf{u}_i^{(m)} + \mathbf{r}_i^{(m)} / a_{ii}^{(m)} \quad \text{for } \mathbf{x}_i \in \Gamma_w. \end{aligned} \quad (14)$$

The next step is to project the predicted values  $\mathbf{u}_i^*$  onto the tangent vector/plane and constrain the corresponding entry of the defect vector  $\mathbf{r}_i^{(m)}$  to be zero

$$\begin{aligned} \mathbf{u}_i^{(m)} &:= \mathbf{u}_i^* - (\mathbf{n}_i \cdot \mathbf{u}_i^*) \mathbf{n}_i, \\ \mathbf{r}_i^{(m)} &:= 0 \quad \text{for } \mathbf{x}_i \in \Gamma_w. \end{aligned} \quad (15)$$

After this manipulation, the corrected values  $\mathbf{u}_i^{(m)}$  act as Dirichlet boundary conditions for the end-of-step solution  $\mathbf{u}_i^{(m+1)}$ . Alternatively, the above projection can be applied to the residual rather than to the velocity vector:

$$\mathbf{r}_i^{(m)} := \mathbf{r}_i^{(m)} - (\mathbf{n}_i \cdot \mathbf{r}_i^{(m)}) \mathbf{n}_i \quad \text{for } \mathbf{x}_i \in \Gamma_w. \quad (16)$$

In either case, there is no overhead cost since the nonlinear algebraic system resulting from an implicit discretization of the Navier-Stokes equations must be solved iteratively anyway. For Cartesian geometries, the modifications to be performed affect just the normal velocity component, as in the case of standard Dirichlet boundary conditions.

### 2.2.3 Wall functions

To complete the problem statement, it remains to prescribe the wall shear stress as well as the boundary conditions for  $k$  and  $\varepsilon$  on  $\Gamma_w$ . Note that the equations of the  $k - \varepsilon$  model are invalid in the vicinity of the wall, where the Reynolds number is rather low and viscous effects are dominant. Therefore, analytical solutions of the boundary layer equations are commonly employed to bridge the gap between the no-slip boundaries and the region of turbulent flow.

The tangential component of the force exerted by the viscous stress tensor  $\sigma = \nu[\nabla\mathbf{u} + \nabla\mathbf{u}^T]$  on  $\Gamma_w$  is given by

$$\mathbf{t}_w = \mathbf{n} \cdot \sigma - (\mathbf{n} \cdot \sigma \cdot \mathbf{n})\mathbf{n}. \quad (17)$$

Note that the velocity vector  $\mathbf{u}$  is tangent to  $\Gamma_w$  due to the free-slip condition  $\mathbf{u} \cdot \mathbf{n} = 0$  imposed on the wall.

The use of logarithmic wall laws leads to the following set of boundary conditions to be prescribed on an internal boundary  $\Gamma_y$  located at a distance  $y$  from the wall  $\Gamma_w$

$$\mathbf{t}_w = -u_\tau^2 \frac{\mathbf{u}}{|\mathbf{u}|}, \quad k = \frac{u_\tau^2}{\sqrt{C_\mu}}, \quad \varepsilon = \frac{u_\tau^3}{\kappa y}, \quad (18)$$

where  $\kappa = 0.41$  is the von Kármán constant. The friction velocity  $u_\tau$  is assumed to satisfy the nonlinear equation

$$\frac{|\mathbf{u}|}{u_\tau} = \frac{1}{\kappa} \log y^+ + \beta \quad (19)$$

valid in the *logarithmic layer*, where the local Reynolds number  $y^+ = \frac{u_\tau y}{\nu}$  is in the range  $11.06 \leq y^+ \leq 300$ . The empirical constant  $\beta$  equals 5.2 for smooth walls.

Theoretically, a boundary layer of width  $y$  should be removed from the computational domain  $\Omega$  and the equations of the  $k - \varepsilon$  model should be solved in the reduced domain. Since  $y^+$  is proportional to  $y$ , the latter should be chosen carefully. It is common practice to apply the wall functions (18) at the first node / integration point located in the interior of the domain. However, the so-defined wall distance  $y$  decreases in the course of mesh refinement and may eventually fall into the viscous sublayer, where the underlying model assumptions are no longer valid.

Another possibility is to adapt the mesh so that the location of boundary nodes always corresponds to a fixed value of  $y^+$  which should be as small as possible for accuracy reasons but large enough to be in the logarithmic layer. Since the deviation from the wall is supposed to remain small, it is worthwhile to neglect it so that no mesh adaptation needs to be performed (Grotjans and Menter, 1998; Lew et-al., 2001). In what follows, the discretized equations will be solved in the original domain  $\Omega$ , whereby the nodes located on the wall  $\Gamma_w$  will be treated in the same way as if they were shifted in the normal direction by the distance  $y$  corresponding to the prescribed  $y^+$ .

As explained in (Grotjans and Menter, 1998), the smallest wall distance for the definition of  $y^+$  corresponds to the point where the logarithmic layer meets the viscous sublayer. At this point, both the linear relation  $y^+ = \frac{|\mathbf{u}|}{u_\tau}$  and equation (19) are assumed to hold. Hence, the optimal value of the parameter  $y^+$  can be found by solving

$$y^+ = \frac{1}{\kappa} \log y^+ + \beta \quad (20)$$

in an iterative way. The resulting solution is given by  $y_*^+ \approx 11.06$  for  $\kappa = 0.41$  and  $\beta = 5.2$  (default settings).

Given a fixed  $y_*^+$  defined as the solution of (20), the friction velocity  $u_\tau$  can be readily computed from

$$u_\tau = \frac{|\mathbf{u}|}{\frac{1}{\kappa} \log y_*^+ + \beta} = \frac{|\mathbf{u}|}{y_*^+}. \quad (21)$$

Remarkably, the nonlinearity and the logarithmic dependence of  $u_\tau$  on  $y^+$  are included in the definition of  $y_*^+$ , so that  $u_\tau = \frac{|\mathbf{u}|}{y_*^+}$  is directly computable. On the other hand, the boundary condition for  $k$  implies that  $u_\tau = C_\mu^{0.25} \sqrt{k}$ . Following (Grotjans and Menter, 1998) we set

$$\mathbf{t}_w = -\frac{u_\tau}{y_*^+} \mathbf{u}, \quad u_\tau = \max \left\{ C_\mu^{0.25} \sqrt{k}, \frac{|\mathbf{u}|}{y_*^+} \right\} \quad (22)$$

which is consistent with (18) and prevents the momentum flux from going to zero at separation/stagnation points.

The resulting natural boundary condition for the wall shear stress is represented by the surface integral

$$\int_{\Gamma_w} (\mathbf{t}_w \cdot \mathbf{w}) ds = - \int_{\Gamma_w} \frac{u_\tau}{y_*^+} (\mathbf{u} \cdot \mathbf{w}) ds, \quad (23)$$

where  $\mathbf{w}$  is the test function for the finite element space.

In view of (18), the boundary value of the turbulent eddy viscosity  $\nu_T$  is proportional to  $\nu$ . Indeed,

$$\nu_T = C_\mu \frac{k^2}{\varepsilon} = \kappa u_\tau y = \kappa y_*^+ \nu. \quad (24)$$

Of course, the above relation is satisfied automatically if the boundary conditions for  $k$  and  $\varepsilon$  are implemented in the strong sense (Kuzmin and Turek, 2004; Turek and Kuzmin, 2005). However, the use of Dirichlet boundary conditions means that the boundary values of  $k$  and  $\varepsilon$  depend solely on the friction velocity  $u_\tau = \frac{|\mathbf{u}|}{y_*^+}$  as a function of  $\mathbf{u}$ . This results in a one-way coupling of the boundary conditions for subproblems (1) and (2)–(3) which is rather unrealistic.

In order to let  $k$  and  $\varepsilon$  ‘float’ and influence the momentum equations via (22)–(23), the wall boundary conditions should be implemented in a weak sense. To this end, let us invoke (18) to retrieve the normal derivatives of  $k$  and  $\varepsilon$  as follows, cf. (Grotjans and Menter, 1998)

$$\begin{aligned} \mathbf{n} \cdot \nabla k &= -\frac{\partial k}{\partial y} = 0, \\ \mathbf{n} \cdot \nabla \varepsilon &= -\frac{\partial \varepsilon}{\partial y} = \frac{u_\tau^3}{\kappa y^2} = \frac{\varepsilon}{y}. \end{aligned} \quad (25)$$

The unknown wall distance  $y$  can be expressed in terms of the turbulent eddy viscosity  $\nu_T = \kappa u_\tau y$ , which yields a natural boundary condition of Newton type

$$\mathbf{n} \cdot \nabla \varepsilon = \frac{\kappa u_\tau}{\nu_T} \varepsilon, \quad u_\tau = C_\mu^{0.25} \sqrt{k}. \quad (26)$$

Hence, the surface integrals associated with the weakly imposed boundary conditions for  $k$  and  $\varepsilon$  are given by

$$\begin{aligned} \int_{\Gamma_w} \frac{\nu_T}{\sigma_k} (\mathbf{n} \cdot \nabla k) w ds &= 0, \\ \int_{\Gamma_w} \frac{\nu_T}{\sigma_\varepsilon} (\mathbf{n} \cdot \nabla \varepsilon) w ds &= \int_{\Gamma_w} \frac{\kappa u_\tau}{\sigma_\varepsilon} \varepsilon w ds. \end{aligned} \quad (27)$$

Alternatively, the right-hand side of the latter equation can be evaluated using the boundary value  $\varepsilon = \frac{u_\tau^3}{\kappa y} = \frac{u_\tau^4}{\kappa y_*^+ \nu}$  as defined by (18), see (Grotjans and Menter, 1998).

Since the resulting boundary values of  $k$  and  $\varepsilon$  are no longer constrained by (18), it is essential to calculate the coefficients  $\nu_T$  and  $P_k$  using the strong form of the wall law. That is, the correct value of the turbulent eddy viscosity is given by (24), while the production term is assumed to be in equilibrium with the dissipation rate, i.e.,

$$P_k = \frac{u_\tau^3}{\kappa y} = \frac{u_\tau^4}{\nu_T} = \frac{u_\tau^4}{\kappa y_*^+ \nu}, \quad (28)$$

where the friction velocity  $u_\tau$  is defined as in equation (22).

### 2.2.4 Chien's Low-Re $k - \varepsilon$ model

The wall functions, as presented above, provide a reasonably good model of the flow behavior in the near-wall region avoiding the need for costly integration to the wall. However, the validity of (18) is limited to flat-plate boundary layers and developed flow conditions (although wall functions are frequently used in other settings with considerable success). Furthermore, the viscous sublayer may occupy a significant portion of the computational domain if the local Reynolds number is relatively small. In this case, the wall distance  $y$  is non-negligible and it is not admissible to apply wall functions on  $\Gamma_w$  rather than on  $\Gamma_y$ .

A more accurate, albeit expensive, approach to the near-wall treatment is provided by numerous Low-Reynolds number  $k - \varepsilon$  models which employ suitable *damping functions* to provide a smooth transition from laminar to turbulent flow. In the framework of the classical Chien model (Chien, 1982), the turbulent eddy viscosity satisfies

$$\nu_T = C_\mu f_\mu \frac{k^2}{\tilde{\varepsilon}}, \quad f_\mu = 1 - \exp(-0.0115y^+), \quad (29)$$

where the dissipation rate  $\varepsilon$  is replaced by the quantity

$$\tilde{\varepsilon} = \varepsilon - 2\nu \frac{k}{y^2}. \quad (30)$$

The above model is supported by the DNS results which indicate that the ratio  $f_\mu = \frac{\nu_T \tilde{\varepsilon}}{C_\mu k^2}$  is not a constant but a function approaching zero at the wall.

The following generalization of equations (4)–(5) is used to compute the  $k$  and  $\tilde{\varepsilon}$  fields (Chien, 1982)

$$\frac{\partial k}{\partial t} + \nabla \cdot \left( k \mathbf{u} - \frac{\nu_T}{\sigma_k} \nabla k \right) + \alpha k = P_k, \quad (31)$$

$$\frac{\partial \tilde{\varepsilon}}{\partial t} + \nabla \cdot \left( \tilde{\varepsilon} \mathbf{u} - \frac{\nu_T}{\sigma_\varepsilon} \nabla \tilde{\varepsilon} \right) + \beta \tilde{\varepsilon} = \gamma C_1 f_1 P_k, \quad (32)$$

where the involved coefficients are given by

$$\begin{aligned} \alpha &= \gamma + \frac{2\nu}{y^2}, \quad \beta = C_2 f_2 \gamma + \frac{2\nu}{y^2} \exp(-0.5y^+), \\ \gamma &= \frac{\tilde{\varepsilon}}{k}, \quad f_1 = 1, \quad f_2 = 1 - 0.22 \exp\left(\frac{k^2}{6\nu\tilde{\varepsilon}}\right). \end{aligned} \quad (33)$$

Chien's model enjoys favorable numerical properties and comes with remarkably simple boundary conditions

$$\mathbf{u} = 0, \quad k = 0, \quad \tilde{\varepsilon} = 0 \quad \text{on} \quad \Gamma_w. \quad (34)$$

Note that the extra sink terms in (31) and (32) have positive coefficients and pose no hazard to positivity of the numerical solution. As before, the linearization parameter  $\gamma$  is recomputed in every outer iteration of the  $l$ -loop. The parameter  $y^+$  depending on the friction velocity  $u_\tau$  is updated at the beginning of the  $k$ -loop as follows

$$y^+ = \frac{u_\tau y}{\nu}, \quad u_\tau = \max \left\{ C_\mu^{0.25} \sqrt{k}, \sqrt{|\mathbf{t}_w|} \right\}, \quad (35)$$

where  $\mathbf{t}_w$  denotes the wall shear stress as defined in (17).

Moreover, the update of  $y^+$  requires knowing the distance to the wall  $y$ . In the current implementation, it is computed in a brute-force way as the distance to the nearest midpoint of a boundary edge/face projected onto the uniquely defined normal associated with this edge/face. Alternatively, the computation of  $y$  can be performed using one of the numerous redistancing/reinitialization techniques developed in the framework of level set methods.

## 3 NUMERICAL EXAMPLES

### 3.1 Channel flow problem

A preliminary validation of Chien's Low-Reynolds number  $k - \varepsilon$  model implemented as explained above was performed on the basis of the well-known channel flow problem. The reference data were provided by the DNS results (Kim et al, 1987) for  $\text{Re}_\tau = 395$  based on the friction velocity  $u_\tau$ , half of the channel width  $d$  and kinematic viscosity  $\nu$ . In order to obtain the developed flow conditions required for validation, the boundary conditions prescribed at the inlet and outlet of the reduced domain were interchanged several times during the computation, so as to emulate periodic boundary conditions in the streamline direction.

The almost mesh-independent solutions displayed in Fig. 1 were obtained using the 3D code on a hexahedral mesh of 50,000 elements. Due to the need for high resolution, local mesh refinement was performed in the near-wall region (see the left diagram). The distance from the wall boundary to the nearest interior point corresponds to  $y^+ \approx 2$ . The right diagram illustrates that the resulting essentially 1D profiles of the nondimensional quantities

$$u^+ = \frac{u_x}{u_\tau}, \quad k^+ = \frac{k}{u_\tau^2}, \quad \varepsilon^+ = \frac{\varepsilon \nu}{u_\tau^4}$$

are in a good agreement with the DNS results (Kim et al, 1987) for this benchmark, whereby the profiles of  $u^+$  and  $\varepsilon^+$  are particularly close to the reference data.

### 3.2 Backward facing step

The second numerical example deals with a turbulent incompressible flow past a backward facing step. The Reynolds number for the 3D simulation to be performed is given by  $\text{Re} = 47,625$  (Ilinca et al., 1998) as defined by the step height  $H$ , mean inflow velocity  $u_{\text{mean}}$  and kinematic viscosity  $\nu$ . The goal is to evaluate the performance of the

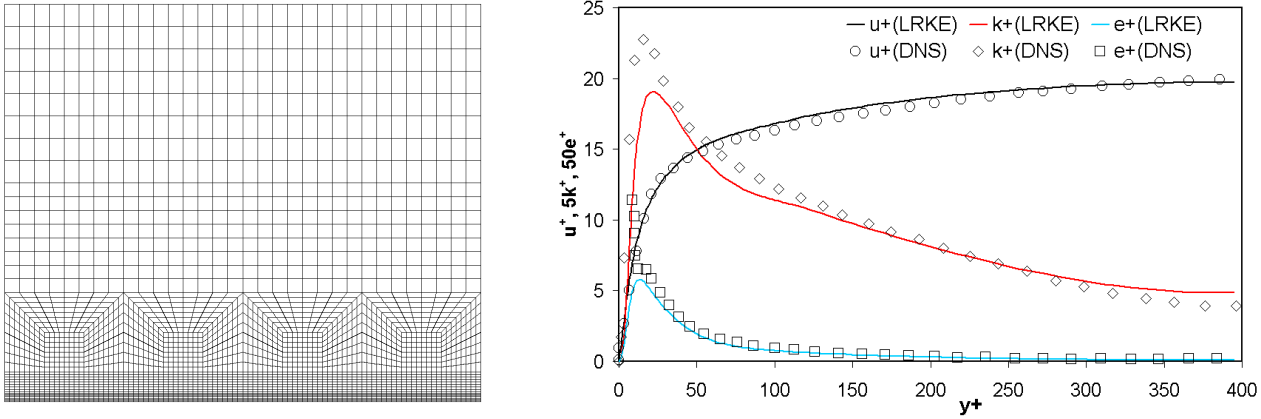


Figure 1: Channel flow: computational mesh and LRKE solutions vs. Kim's DNS results for  $Re_\tau = 395$ .

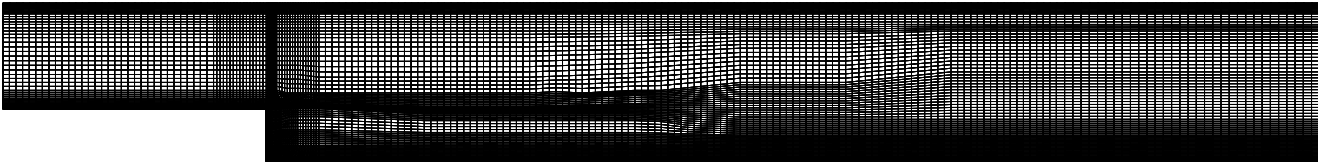


Figure 2: Backward facing step: a two-dimensional view of the computational mesh in the  $xy$ -plane.

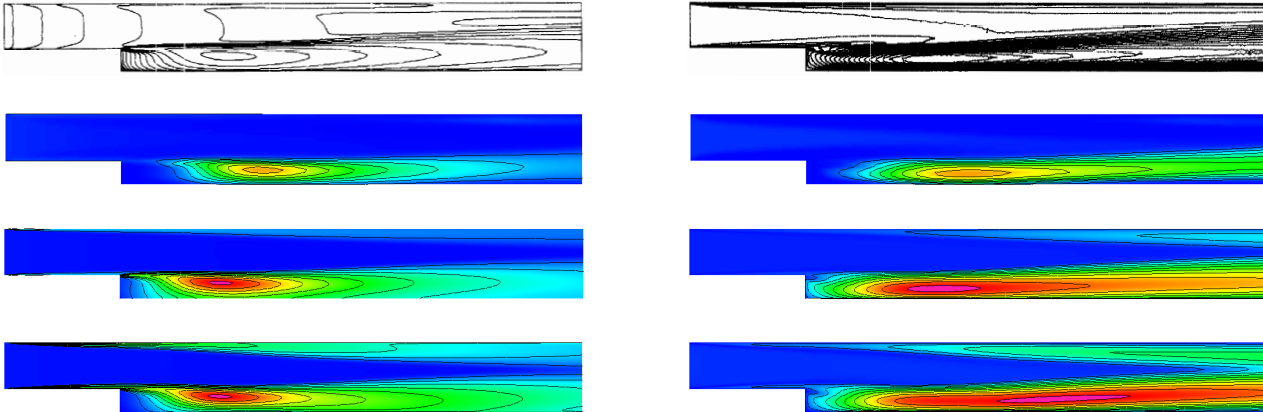


Figure 3: Backward facing step: steady-state distribution of  $k$  (left) and  $\nu_T$  (right) for  $Re = 47,625$ . From top to bottom: reference solution (Ilinca et-al., 1998), wall functions implemented as Dirichlet boundary conditions, wall functions implemented as Neumann boundary conditions, and Chien's Low-Reynolds number modification.

standard  $k - \varepsilon$  model with three different kinds of near-wall treatment: wall functions implemented as Dirichlet (DIRBC) and Neumann (NEUBC) boundary conditions vs. Chien's Low-Reynolds number version (LRKE).

All simulations were performed on the same computational mesh consisting of approximately 260,000 elements, see Fig. 2. Local mesh refinement was employed in the vicinity of the walls and in the shear layer behind the step. A comparison of the steady-state solutions for the turbulent kinetic energy  $k$  and eddy viscosity  $\nu_T$  with the reference solution from (Ilinca et-al., 1998) is presented in Fig. 3. Significant differences between the solutions

computed using wall functions implemented in the strong and weak sense are observed even in the 'picture norm'. The use of Dirichlet boundary conditions (DIRBC) for  $k$  and  $\varepsilon$  was found to produce rather disappointing results, whereas the performance of Neumann boundary conditions (NEUBC) is very similar to that of the Low-Reynolds number  $k - \varepsilon$  model (LRKE) under investigation.

An important evaluation criterion for this popular test problem is the recirculation length defined as  $L_R = x_r/H$ . For the implementation based on wall functions implemented as Dirichlet boundary conditions, this integral quantity can be readily inferred from the distribution of

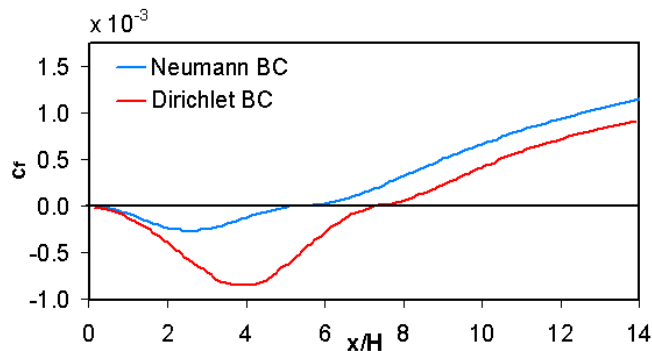


Figure 4: Backward facing step: distribution of the skin friction coefficient  $c_f$  along the lower wall,  $Re = 47,625$ .

the skin friction coefficient  $c_f = \frac{u_z^2}{u_{mean}^2} \frac{u_x}{|u_x|}$  on the bottom wall (see Fig. 4). The recirculation length predicted by Chien’s Low-Re  $k - \varepsilon$  model and by wall functions with Neumann boundary conditions (27) is underestimated ( $L_R \approx 5.4$ ), which is also the case for the computational results published in the literature ( $5.0 < L_R < 6.5$ , see (Ilinca et-al., 1998; Grotjans and Menter, 1998; Thangam and Speziale, 1992)). On the other hand, the implementation of wall functions in the strong sense yields  $L_R \approx 7.1$ , which matches the experimentally measured recirculation length  $L_R \approx 7.1$ , see (Kim, 1978). Unfortunately, this perfect agreement turns out to be a pure coincidence.

In Fig. 5, the calculated velocity profiles for 6 different distances from the step are compared to one another and to the experimental data from Kim’s thesis (Kim, 1978). The corresponding profiles of  $k$  and  $\varepsilon$  are displayed in Fig. 6 and Fig. 7, respectively. This comparative study indicates that the  $k - \varepsilon$  model equipped with wall functions implemented as Neumann boundary conditions yields essentially the same results as its Low-Reynolds number counterpart, whereas the use of Dirichlet boundary conditions leads to a significant discrepancy, especially at small distances from the step. It is also worth mentioning that the presented profiles of  $\varepsilon$  do not suffer from spurious undershoots which are frequently observed in other computations. This can be attributed to the positivity-preserving discretization of convective terms which is explained in detail elsewhere (Kuzmin and Möller, 2005; Kuzmin, 2006).

#### 4 CONCLUSIONS

Finite element discretization and iterative solution techniques were presented for the incompressible Navier-Stokes equations coupled with the  $k - \varepsilon$  turbulence model. Various approaches to the near-wall treatment were discussed in detail. The presented numerical study illustrates the utility of ‘scalable’ wall functions (Grotjans and Menter, 1998) implemented as natural boundary conditions. The accuracy of simulation results is comparable to that provided by Chien’s Low-Re  $k - \varepsilon$  model on the same mesh.

#### REFERENCES

- Chien K.-Y. (1982) ‘Predictions of Channel and Boundary-Layer Flows with a Low-Reynolds-Number Turbulence Model.’, *AIAA J.* **20**, pp.33-38.
- Codina R. and Soto O. (1999) ‘Finite Element Implementation of Two-Equation and Algebraic Stress Turbulence Models for Steady Incompressible Flows.’ *Int. J. Numer. Methods Fluids* **30** pp.309-333.
- Engelman M. S., Sani R. L. and Gresho P. M. (1982) ‘The Implementation of Normal and/or Tangential Boundary Conditions in Finite Element Codes for Incompressible Fluid Flow.’ *Int. J. Numer. Meth. Fluids* **2** pp.225-238.
- Grotjans H. and Menter F. (1998) ‘Wall Functions for General Application CFD Codes.’, *ECCOMAS 98, Proceedings of the 4th Computational Fluid Dynamics Conference*, John Wiley & Sons, pp.1112-1117.
- Ilinca F., Héту J.-F. and Pelletier D. (1998) ‘A Unified Finite Element Algorithm for Two-Equation Models of Turbulence.’, *Comp. & Fluids* **27-3** pp.291-310.
- Kim J. (1978) ‘Investigation of Separation and Reattachment of Turbulent Shear Layer: Flow over a Backward Facing Step.’, *PhD Thesis*, Stanford University.
- Kim J., Moin P. and Moser R. D. (1987) ‘Turbulence Statistics in Fully Developed Channel Flow at Low Reynolds Number.’, *J. Fluid Mech.*, **177** pp.133-166.
- Kuzmin D. (2006) ‘On the Design of General-Purpose Flux Limiters for Implicit FEM with a Consistent Mass Matrix.’ *J. Comput. Phys.* **219** pp.513-531.
- Kuzmin D. and Möller M. (2005) ‘Algebraic Flux Correction I. Scalar Conservation Laws’, In: Kuzmin D., Löhner R. and Turek S. (eds.) *Flux-Corrected Transport*, Springer, pp.155-206.
- Kuzmin D. and Turek S. (2004) ‘Multidimensional FEM-TVD Paradigm for Convection-Dominated flows.’, In: *ECCOMAS 2004. Proceedings of the IV European Congress on Computational Methods in Applied Sciences and Engineering*, Volume II, ISBN 951-39-1869-6.
- Lew A. J., Buscaglia G. C. and Carrica P. M. (2001) ‘A Note on the Numerical Treatment of the  $k - \varepsilon$  Turbulence Model.’, *Int. J. of Comp. Fluid Dyn.* **14**, pp.201-209.
- Medić G. and Mohammadi B. (1999) ‘NSIKE - an Incompressible Navier-Stokes Solver for Unstructured Meshes.’ *INRIA Research Report* **3644**.
- Thangam S. and Speziale C. G. (1992) ‘Turbulent Flow Past a Backward-Facing Step: A Critical Evaluation of Two-Equation Models.’, *AIAA J.* **30-5**, pp.1314-1320.
- Turek S. and Kuzmin D. (2005) ‘Algebraic Flux Correction III. Incompressible Flow Problems’, In: Kuzmin D., Löhner R. and Turek S. (eds.) *Flux-Corrected Transport*, Springer, pp.251-296.

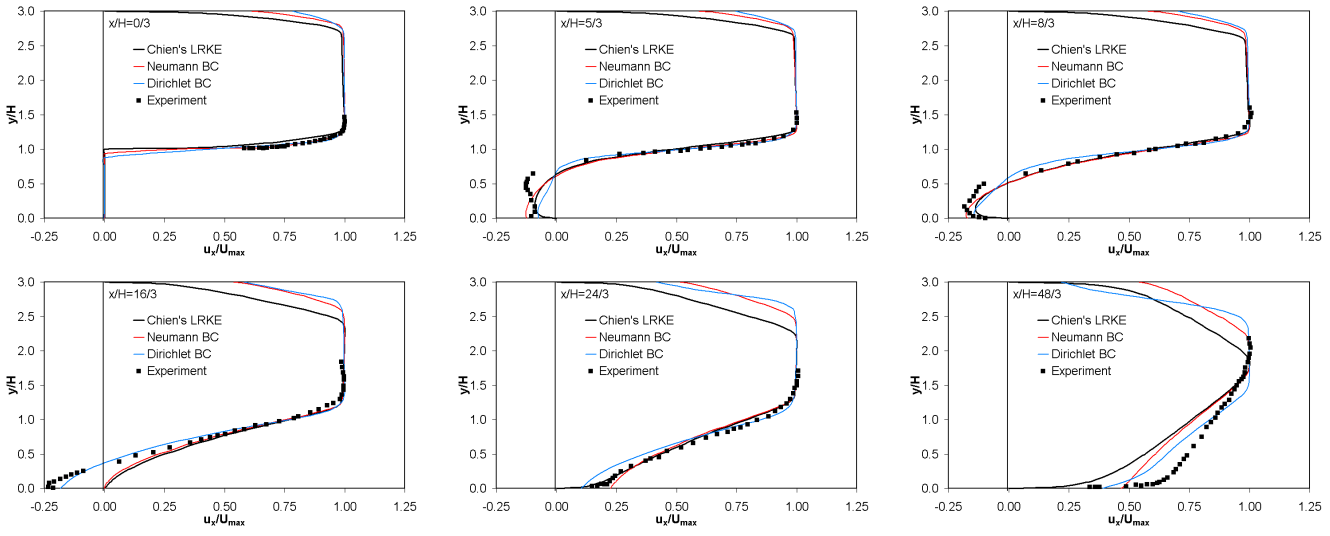


Figure 5: Backward-facing step: velocity profiles  $u_x$  for 6 different distances  $x/H$  from the step. Solutions computed using the  $k - \varepsilon$  model with three different kinds of near-wall treatment vs. experimental data (Kim, 1978).

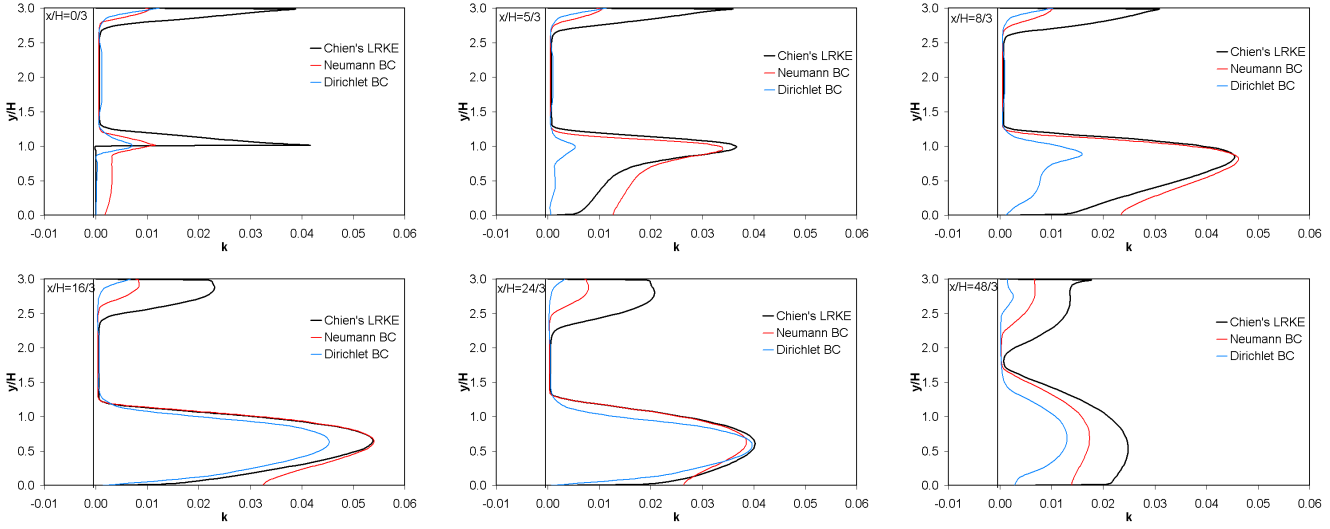


Figure 6: Backward-facing step: turbulent kinetic energy  $k$  for 6 different distances  $x/H$  from the step.

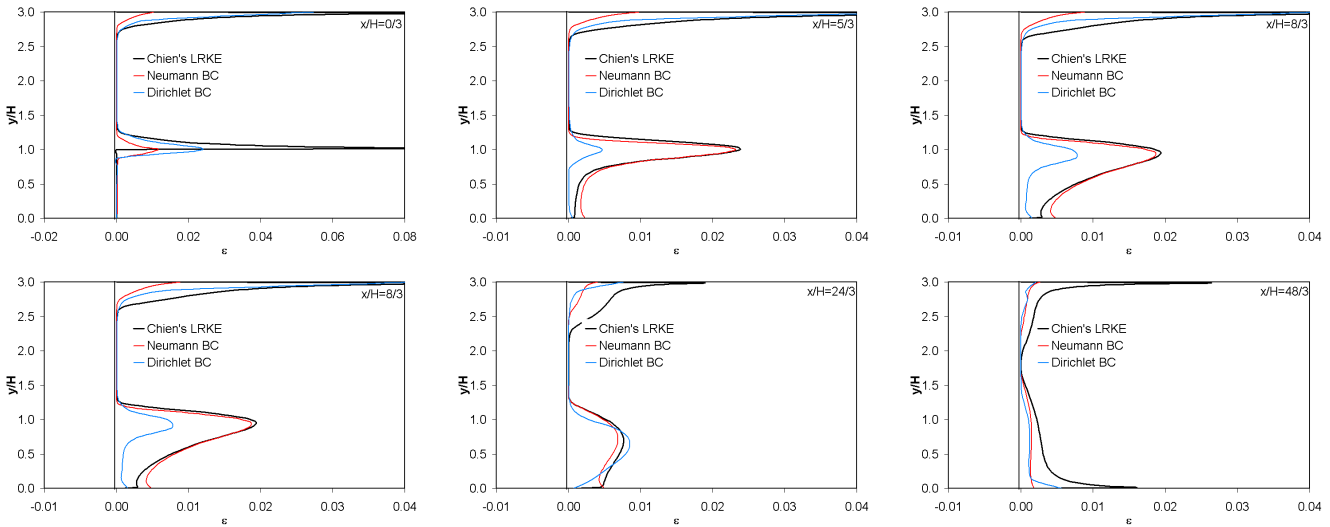


Figure 7: Backward-facing step: dissipation rate  $\varepsilon$  for 6 different distances  $x/H$  from the step.